Inorganic Chemistry

ARTICLE

pubs.acs.org/IC

New Fe^{3+}/Cr^{3+} Perovskites with Anomalous Transport Properties: The Solid Solution $La_xBi_{1-x}Fe_{0.5}Cr_{0.5}O_3$ ($0.4 \leq x \leq 1$)

M. E. Villafuerte-Castrejón,[†,‡] M. García-Guaderrama,[§] L. Fuentes,[⊥,‡] J. Prado-Gonjal,[‡] A. M. González,[∥] M. Á. de la Rubia,[∥,▽] M. García-Hernández,[¶] and E. Morán[‡,*]

[†]Instituto de Investigaciones en Materiales, Universidad Nacional Autónoma de México, AP 70360 México DF 04510, México

[⊥]Centro de Investigación en Materiales Avanzados SC, Complejo Industrial Chihuahua, M. Cervantes 120, Chihuahua 31109, México

[§]Centro de Investigación en Materiales DIP-CUCEI, Universidad de Guadalajara, Av. Revolución 1500, Col. Olímpica, Guadalajara, México

[‡]Departamento de Química Inorgánica, Facultad de Ciencias Químicas, UCM, 28040 Madrid, Spain

[∥]Grupo Poemma, Technical University of Madrid, ETSI Telecomunicación, Ctra. Valencia km 7, 28031 Madrid, Spain

[¶]Instituto de Ciencia de Materiales de Madrid, CSIC, Cantoblanco, 28049 Madrid, Spain

ABSTRACT: In this work, the sol−gel synthesis, structural characterization, and transport properties of a new solid solution of the general formula $La_xBi_{1-x}Fe_{0.5}Cr_{0.5}O_3$ ($0.4 \leq x \leq 1$) are presented. The solubility limit x has been determined and variation of the lattice parameters measured through profile fitting. The cell parameters, space group, and atomic positions, as obtained by the Rietveld refinement of X-ray diffraction data, are reported. This analysis and electron diffraction studies as well do not reveal any evidence of Fe/Cr ordering. Regarding the transport properties, magnetic and electric characterizations are described. The electrical response with the temperature and frequency has been studied, and a "positive temperature coefficient" for the resistivity has been found for temperatures between 270 and 400 °C. The magnetic behavior is striking because, for all materials studied, zero-field-cooling curves appear above field-cooling ones, an anomalous feature that is interpreted as being due to complex ferromagnetic/antiferromagnetic interactions in the B perovskite sublattice.

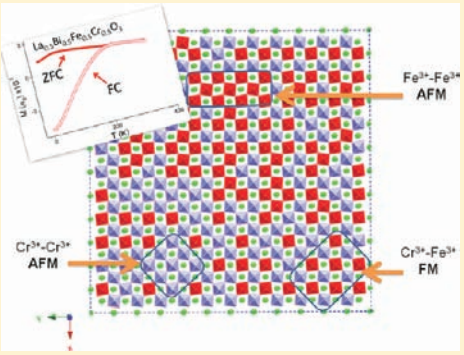

INTRODUCTION

In recent years, double perovskites of the general formula $A_2BB'O_6$, where Fe^{3+} and Cr^{3+} are located in the B and B′ sites are under focus on the search for multifunctional materials. According to the Kanamori−Goodenough rules, these cations, if ordered in an adequate way, would produce a nonconducting, ferromagnetic (FM) material because of superexchange interactions between these cations, the electronic configurations of which are $t_{2g}^3e_g^2$ (Fe^{3+}) and $t_{2g}^3e_g^0$ (Cr^{3+}), respectively.[1,2] In this connection, the structure and properties of double perovskites with composition A_2FeCrO_6 (A = La^{3+}, Y^{3+}) have been reported.[3,4] It is worth noting that Azad et al.[3] have studied by neutron powder diffraction the structural and magnetic properties of $LaFe_{0.5}Cr_{0.5}O_3$ and shown that the structure is an orthorhombic, $GdFeO_3$ type (space group *Pbnm*), with random positioning of the Fe and Cr cations in the B sublattice, the same structure featured by the simple perovskites $LaCrO_3$ and $LaFeO_3$. Indeed, Ueda et al.[5] have achieved an FM spin order in superlattices consisting of alternating layers of $LaCrO_3$ and $LaFeO_3$ along the [111] direction.

Regarding magnetism, the end members of the series have also been explored, with both being antiferromagnetically ordered with T_{Neel} = 280 and 750 K, respectively. In a similar way, neutron diffraction and magnetization data for $LaFe_{0.5}Cr_{0.5}O_3$ reveal an overall antiferromagnetic (AFM) behavior with uncompensated spins near the Neel temperature (G-type structure, T_{Neel} = 265 K), showing weak magnetization at low temperatures.[3] Nevertheless, in spite of these similarities, the magnetic properties of the Fe/Cr mixed La perovskite are puzzling and, contrary to what is usually found, the zero-field-cooling (ZFC) curve lies above the field-cooling (FC) one, something not well understood, yet.

On the other hand, introducing a lone-pair cation such as Bi^{3+} in the cuboctahedral A site of Fe/Cr perovskite oxides is extremely interesting because of the prediction made by Baettig and Spaldin[6,7] based on first-principles calculations. According to these authors, the hypothetical double perovskite Bi_2FeCrO_6, where Fe^{3+}/Cr^{3+} should be long-range-ordered, would have a magnetic moment of 2 μ_B per formula unit and a polarization of ≈80 μC/cm, being then multiferroic. Interestingly, a new material with this desired composition has already been prepared by Suchomel et al.[8] working under high-pressure/high-temperature conditions (6 GPa and 1000 °C), but Fe^{3+} and Cr^{3+} are

Received: April 27, 2011
Published: July 25, 2011

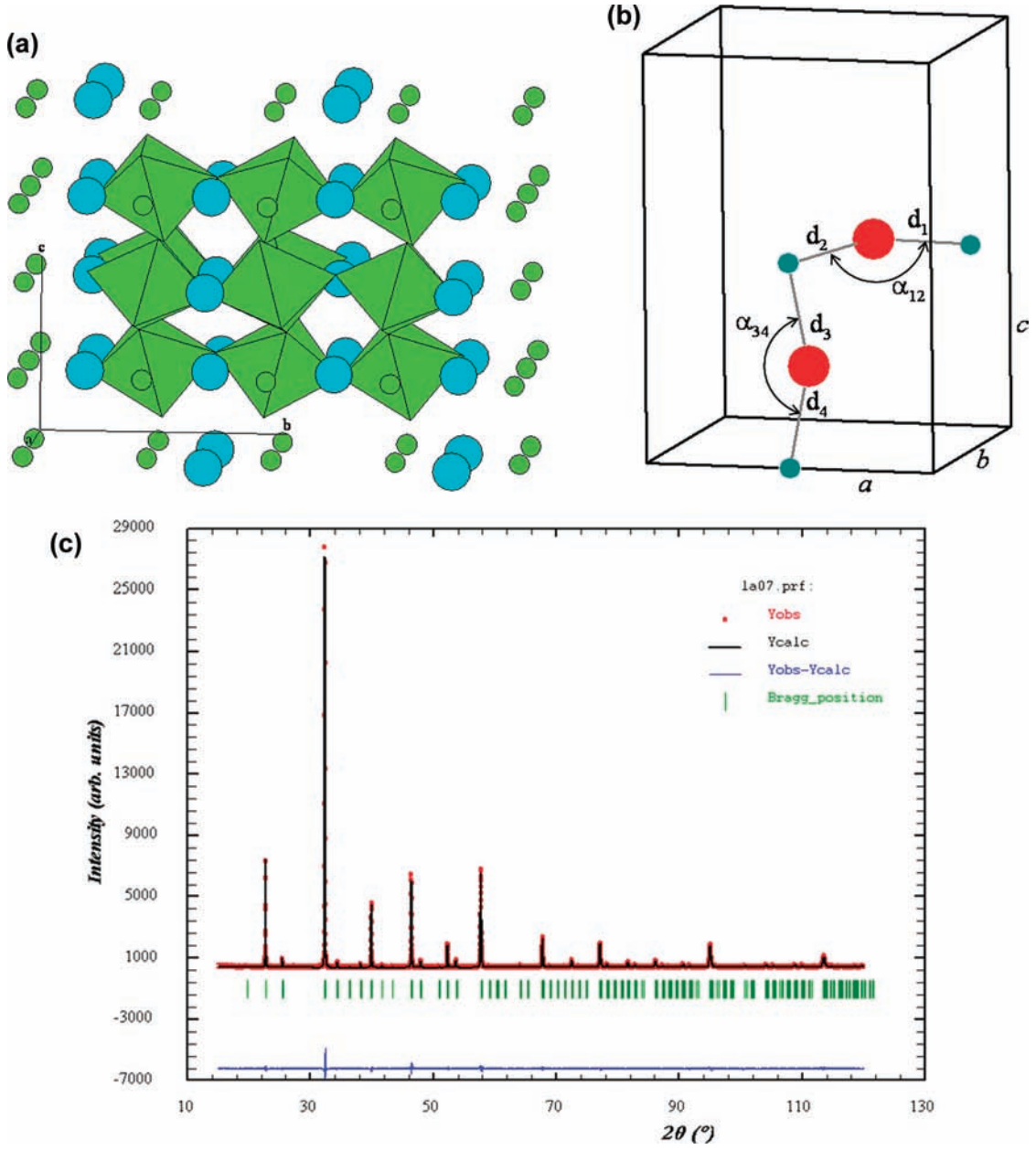

Figure 1. Crystallographic characterization of $Bi_{0.5}La_{0.5}Fe_{05}Cr_{0.5}O_3$: (a) Schematic crystal structure of the $Bi_{1-x}La_xFe_{05}Cr_{0.5}O_3$ solid solution space group (*Pbnm*). Octahedral tilting is evident. Bigger spheres correspond to A cations (Bi or La); smaller ones denote B cations (Fe or Cr). (b) Orthorhombic unit cell. Selected bond angles and distances are shown. (c) XRD Rietveld refinement of $Bi_{0.5}La_{0.5}Fe_{05}Cr_{0.5}O_3$. Observed (red) and calculated (black). $\chi^2 = 1.40$. The observed and calculated profiles are shown.

completely disordered on the B site; this results in a conventional, not multiferroic, material with paramagnetic behavior at room temperature. $T_{Néel}$ is strongly depleted to 130 K, probably because of antisite disorder in the B sublattice. Other authors have reported the synthesis of this material by a combustion method, claiming to obtain an FM material, but the samples, through careful examination of the powder X-ray diffraction (XRD) patterns, seem to be impurified by a secondary phase, maghemite-like, a well-known ferrimagnetic material.[9] To our knowledge, there are no reports on Bi^{3+}/La^{3+} substitution in $LaFe_{0.5}Cr_{0.5}O_3$, although the solid solutions $La_{1-x}Bi_xCrO_3$ ($x < 0.35$) and $La_{1-x}Bi_x$ FeO_3 ($0 < x < 1$) have been described, respectively. It is worth noting that Guo et al.[10] found that including Bi^{3+} in the $LaCrO_3$ structure results in electric polarizations that are dependent on the Bi^{3+} concentration and Chen et al.[11] reported on structural and specific heat data.

Taking all this into account, the aim of this work was to prepare new materials of composition $La_xBi_{1-x}Fe_{0.5}Cr_{0.5}O_3$, to determine the solid solution range ($0.4 \leq x \leq 1$), and to explore their structural, electrical, and magnetic properties. The synthesis of very pure polycrystalline powders has been successfully achieved at room pressure by a sol−gel method, and although the structure is quite simple, the transport properties appear to be intriguingly complex, especially in which concerns the magnetic properties, where ZFC curves are found to lie above the corresponding FC ones, a feature rarely observed.[3,12,13] Among

dx.doi.org/10.1021/ic2008864 |*Inorg. Chem.* 2011, 50, 8340–8347

other interesting results found for these materials, it is worth pointing out that they exhibit a semiconductor behavior with a temperature region of a "positive temperature coefficient" (PTC) for the resistivity. This can be potentially applied in devices such as temperature sensors or controllers, protection elements in circuits, or self-regulation smart devices;[14] actually, lead-free PTC resistors are already being used for such applications.

EXPERIMENTAL SECTION

Samples were prepared by mixing and milling the appropriate amounts of $Bi(NO_3)_3 \cdot 5H_2O$, $La(NO_3)_3 \cdot 6H_2O$, $Fe(NO_3)_3 \cdot 9H_2O$, and $Cr(NO_3)_3 \cdot 9H_2O$ (all of them analytical-grade reactants purchased from Sigma-Aldrich). $CH_3O-CH_2-CH_2OH$ (2-methoxyethanol) was added until complete dissolution of the reactants and then slowly evaporated under agitation at 80 °C until the mixture was completely dried, forming the gels. In each case, the gel was then ground into powder, followed by calcination at 900 °C for 12 h. For preliminary structural characterization, X-ray data were collected on a X'Pert MPD Philips diffractometer, with Cu $K\alpha_1$ radiation obtained with a Cu-curved monochromator, at 45 kV and 40 mA. For Rietveld analysis, a Philips X'Pert PRO ALPHA1 of Panalytical BV instrument with Cu $K\alpha_1$ radiation with a primary curved Ge111 monochromator and a speed X'Celerator detector was employed. The angular interval and step were $5.000° < 2\theta < 120.000°$ and $\Delta(2\theta) = 0.008°$. *Fullproof* software[15] was used for profile fittings, cell parameters, and general Rietveld refinement. In order to examine whether some structural changes occur during heating, an automatic Philips X'Pert PRO diffractometer with a $\theta-\theta$ configuration, fitted with Cu $K\alpha_1$ radiation and an Anton Paar HTK1200 high-temperature camera, with a Pt sample holder and working in air, was used. Thermal analysis (TGA and DTA) was performed on a Perkin-Elmer Pyris setup.

In the search for possible superstructures, selected area electron diffraction (SAED) was performed in a JEOL 2000FX electron microscope operating at 200 kV. Sample morphologies and grain sizes were examined by means of scanning electron microscopy (SEM) on a JEOL 6400 microscope equipped with an EDAX Inc. energy-dispersive X-ray detector for microanalysis.

The magnetic properties of the as-prepared powder samples have been measured in a Squid magnetometer, manufactured by Quantum Design, equipped with a 7 T superconducting coil. The temperature dependence of the magnetization has been measured following zero-field-cooling—field-cooling (ZFC—FC) protocols. Hysteresis cycles have been also recorded at several temperatures.

Aiming to know the electric and dielectric properties of these new materials, permittivity and conductivity measurements have been performed, as a function of the temperature and frequency, using well-sintered (air, 950—1040 °C, 12 h), disk-shaped pellets (~1 mm thickness and 10 mm diameter). Pt electrodes were deposited by a BAL-TEC SCD 050 sputter coater on the parallel faces of the pellets. Samples were then placed inside a well-controlled vertical furnace, which was set at thermal equilibrium prior to each frequency run. For electrical measurements, we took complex impedance spectra of samples for frequencies in the range from 1 kHz to 12 MHz using a 4194A impedance/gain-phase analyzer from Agilent to get both the magnitude and phase of the admittance under a stimulating signal (oscillator level) of 0.5 V_{rms}. Materials were studied in the interval between room temperature and 600 °C; during heating, we took scans for the frequency range at selected temperatures to try to get the best accuracy in the regions where the greater variations in the impedance appear, paying special attention to stabilization of the temperature and avoiding the concurrence of a current peak in the oven during scanning. Thus, for each sample, we obtained a double scan, in frequencies and temperatures.

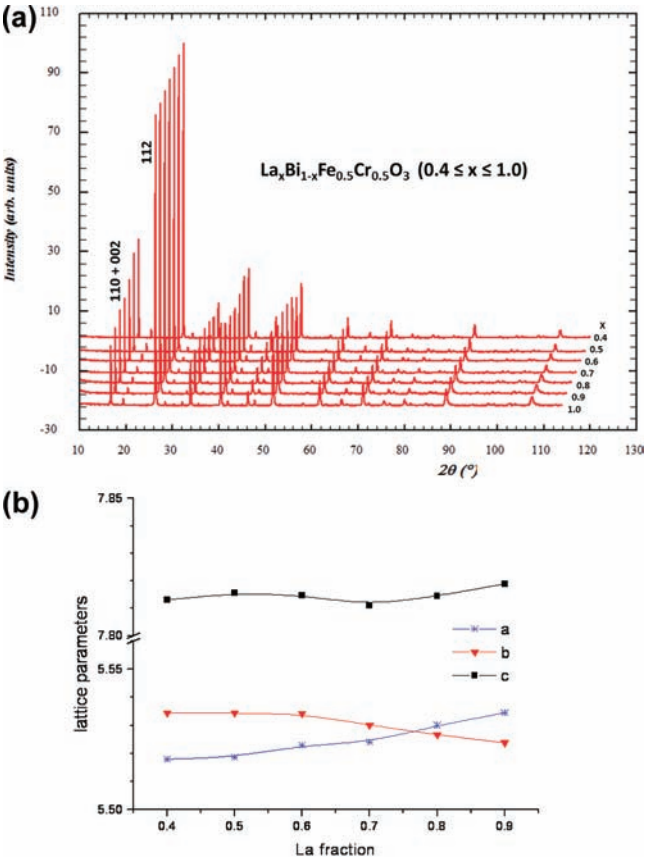

Figure 2. X-ray characterization of the solid solution: (a) XRD patterns of the solid solution specimens; (b) cell parameters as a function of the La/Bi substitution degree.

RESULTS AND DISCUSSION

A new solid solution with formula $La_xBi_{1-x}Fe_{05}Cr_{0.5}O_3$ ($0.4 < x < 1$) has been synthesized, as described above in the Experimental Section, and in this connection, it is worth pointing out that methoxyethanol plays an essential role because it is one of the few solvents able to form a sol with bismuth nitrate. The samples were characterized at several levels.

a. Structure: Powder XRD. The structural model used for the Rietveld refinement was the orthorhombic $GdFeO_3$ structure (ICSD no. 172009),[16] which holds both for one of the existing $LaCrO_3$ polymorphs (ICSD no. 91270)[17] and for $LaFeO_3$ (ICSD no. 28255).[18] The orthorhombic perovskite structure [space group *Pbnm* (No. 62)], featuring characteristic octahedral tilting, is shown in Figure 1a. The diagonal unit cell ($a \approx b \approx a_p\sqrt{2}$; $c \approx 2a_p$) showing important angles and metal—oxygen distances is schematized in Figure 1b. As the most representative example, the Rietveld refinement of $La_{0.5}Bi_{0.5}Fe_{05}Cr_{0.5}O_3$ is shown in Figure 1c: no signs of ordering, either in the A sites or in the B ones, are detected; figures of merit are $R_{wp} = 9.97$ and $\chi^2 = 1.26$. It is worth noting that this structure is quite different from that of rhombohedral $BiFeO_3$ (space group $R3\overline{m}$, ICSD no. 157424);[19] thus, important structural changes are expected for lower degrees of substitution (that is, higher Bi^{3+} contents), which may be the cause for the fact that, using our synthetic procedure, only mixtures of phases are obtained for $x < 0.4$, this being the lower limit of the solid solution range. Therefore, the Bi^{3+} *lone-pair effect* appears to drive important structural changes.

Table 1. XRD Results As Obtained from Rietveld Analysis

	nominal "x" in $La_x Bi_{1-x}Cr_{0.5}Fe_{0.5}O_3$ (space group *Pbnm*)						
	0.4	0.5	0.6	0.7	0.8	0.9	1.0
a (Å)	5.5180(1)	5.5186(1)	5.5229(1)	5.5240(1)	5.5300(2)	5.5344(2)	5.5388(1)
b (Å)	5.5344(1)	5.5343(1)	5.5341(1)	5.5301(1)	5.5267(2)	5.5238(2)	5.5220(1)
c (Å)	7.8130(1)	7.8156(1)	7.8148(1)	7.8110(1)	7.8145(2)	7.8189(2)	7.8171(2)
f(La occ.)	0.42(1)	0.54(1)	0.68(1)	0.76(1)	0.85(1)	0.97(1)	1.00
density (g/cm^3)	7.78	7.55	7.28	7.12	6.94	6.71	6.57
$B(O_1) = B(O_2)$	1.4(1)	1.3 (1)	1.2(1)	1.5(1)	0.9(2)	1.0(2)	1.0(2)
R_{wp}	6.39	9.97	5.78	4.86	5.12	5.39	4.80
χ^2	1.38	1.26	1.50	1.13	1.07	1.46	1.26

On the other hand, the fact that ionic radii of the A^{3+} cations (La and Bi) are quite similar[20] accounts for the observed random distribution in the A site.

Figure 2a shows the experimental powder XRD patterns corresponding to different members of the solid solution. The intensities are normalized relative to the most intense (112) peak. The measured diffraction patterns exhibit the characteristic Bragg reflections corresponding to the above-mentioned $GdFeO_3$ orthorhombic perovskite over the whole solid solution range. A systematic variation of the peak intensities is observed upon La/Bi substitution: the higher the contents of La^{3+}, the lower the intensity of the (110 + 002) doublet. Table 1 shows a summary of the crystallographic results obtained by Rietveld refinements together with the corresponding densities. The cell parameter variations are shown in Figure 2b, and Table 2 shows selected interatomic O−B−O distances and angles. Some observed regularities are the following: as a general comment, La/Bi substitution leads to slight, although regular, changes in the structural parameters, without symmetry changes or other qualitative transformations, something that can be explained on the basis of similar ionic radii. The a parameter slightly increases, b slightly decreases, and c remains almost constant. Variations produced in the O−B−O distances and angles upon substitution in the A site are also weak (see Table 2). Careful inspection of the distance and angle variations leads to recognition of a correlation among these geometrical features and the unit cell geometrical parameters. Distances d_1 and d_2 are mostly linked with variations in a and b lattice parameters, while d_3 and d_4 are correlated basically with variations in c. All of these distances, ranging from 1.95 to 2.03 Å, correlate quite well with the sum of the corresponding ionic radii: average radius for $^{VI}B^{3+}$ = 0.63 Å; $^{II}O^{2-}$ radius = 1.35 Å.[17]

Regarding the degrees of substitution achieved, La^{3+} concentrations are well determined from peak intensities, as reported in Table1. Chemical compositions obtained from the experimentally refined data are similar to the nominal ones. The "diffraction" f occupation factors for La^{3+} are systematically higher than the nominal ones. This (small) systematic error may be due to texture or anomalous scattering, among other effects.

b. Microstructure: SEM Images. As a representative example, two micrographs corresponding to the $Bi_{0.5}La_{0.5}Fe_{05}Cr_{0.5}O_3$ sample are shown: the as-prepared material (Figure 3a) and after being sintered at 1040 °C (Figure 3b). The as-prepared powder samples are made of grains with polyhedral shapes and sizes ranging from 1 to 3 μm. The sintered samples, for compositions of $0.5 \leq x \leq 0.7$, show larger sized (up to 6 μm) rounded grains, with good contact between them, as required for electrical measurements.

Table 2. Interatomic Distances (Å) and Angles (deg) (see Figure 1b)

	nominal La^{3+} contents x					
	0.4	0.5	0.6	0.7	0.8	0.9
d_1	2.00	2.01	2.03	2.01	1.97	1.96
d_2	1.99	1.97	1.96	1.97	1.99	2.01
α_{12}	157	157	157	158	160	158
$d_3 = d_4$	2.01	2.00	2.00	2.00	2.01	2.00
α_{34}	153	155	155	156	152	155

Energy-dispersive spectrometry (EDS) microanalysis was performed in situ for all samples both in an average mode and also by the selection of single particles. The results are shown in Figure 3c, and the compositions observed are in reasonable agreement with the nominal ones either before or after sintering.

c. Transmission Electron Microscopy and Electron Diffraction. SAED patterns corresponding to different samples along different zone axes are shown in Figure 4. All of them can be indexed within the space group *Pbnm* (No. 62) and with lattice parameters close to $a \sim b \sim 5.5$ Å and $c \sim 7.8$ Å, which is in good agreement with the previously reported XRD results. No superstructure spots are detected in any case, meaning that both the A cations (Bi/La) and the B ones (Fe/Cr) are randomly disordered in the corresponding sublattices, also in full agreement with the X-ray observations. EDS analysis performed in situ confirms in all cases the nominal compositions.

d. Electrical Properties. In order to check the electric behavior of these materials, their electrical conductivity, σ, and the real part of the permittivity, εR, have been measured from room temperature up to 500 °C. First, we noticed a remarkable difference between different samples depending on the sintering conditions used. Aiming to avoid misinterpretations due to these differences, we chose three compositions (La = 0.5, 0.6, and 0.7), all of them sintered at optimal conditions (air, 950 °C, 12 h). This temperature is close to the peritectic melting point (rounded grains), and higher temperatures and/or longer times result in partial decomposition of the samples because Fe/Cr maghemite octahedral particles are evident by SEM and some bismuth oxide is volatilized. Experimental densities of the pellets corresponding to these compositions, estimated by geometrical and weighing means, are above 90% of the calculated ones, indicating that a high degree of sintering is also evident in the SEM micrographs

dx.doi.org/10.1021/ic2008864 |*Inorg. Chem.* 2011, 50, 8340–8347

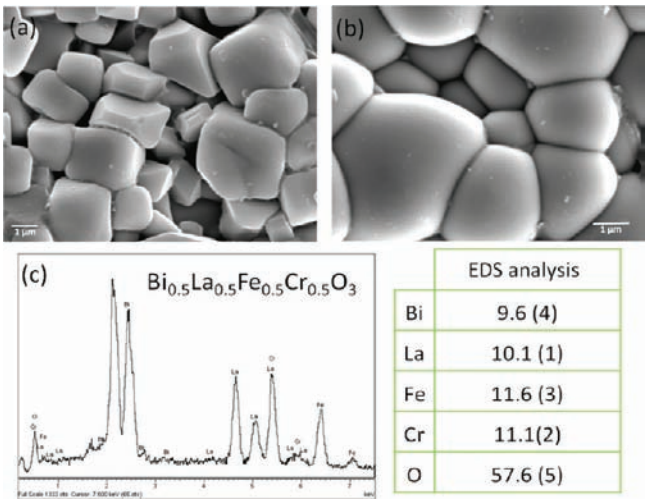

	EDS analysis
Bi	9.6 (4)
La	10.1 (1)
Fe	11.6 (3)
Cr	11.1(2)
O	57.6 (5)

Figure 3. SEM micrographs corresponding to the $Bi_{0.5}La_{0.5}Fe_{05}Cr_{0.5}O_3$ sample: (a) as-prepared; (b) sintered at 1040 °C; (c) EDS microanalysis.

(e.g., for $Bi_{0.3}La_{0.7}Fe_{0.5}Cr_{0.5}O_3$). Figure 5 plots the real part of the permittivity as a function of the temperature, and Figure 6 gives conductivity−temperature plots for these samples. A significant parallelism is evident. For both of them, we found similar behavior: they exhibit a continuous increase up to 300 °C and a sudden fall after this temperature; a strong dependence on the La^{3+} content also exists, and this effect seems to be stronger as the amount of La^{3+} decreases. These materials exhibit semiconductor behavior, as we observe in the conductivity−temperature plot (Figure 6) for temperatures below 270 °C and over 400 °C. It is worth noting that for each composition we found a region with a PTC for the resistivity, $\rho = 1/\sigma$, that might correspond to grain boundary conduction, as reported by other authors in compounds based on the $BaTiO_3$ semiconductor ceramics.[21] Lead-free PTC resistors are used in devices as temperature sensors and controllers, heaters, overheating or electric shock protection, and smart control devices.[22] We have observed a shift in the region of a PTC upon going to lower temperature ranges with increasing La content (300−440 °C for $Bi_{0.5}La_{0.5}Fe_{0.5}Cr_{0.5}O_3$, 28−380 °C for $Bi_{0.4}La_{0.6}Fe_{0.5}Cr_{0.5}O_3$, and 260−340 °C for $Bi_{0.3}La_{0.7}Fe_{0.5}Cr_{0.5}O_3$).

Aiming to know whether or not this electrical effect was associated with a phase transition, we performed DTA measurements—up to 900 °C—and XRD at 500 °C for the $x = 0.5$ sample, well above the temperature at which the PTC feature is observed. Thermal analysis does not show any evidence of transition, and the corresponding high-temperature diffraction pattern does not show significant differences with regard to the room temperature pattern: the space group is the same (*Pbnm*) and, as expected, the cell parameters increase isotropically; a = 5.5566(4) ($\Delta \sim 0.6\%$), b= 5.55684(5) ($\Delta \sim 0.6\%$), and c = 7.8602(6) ($\Delta \sim 0.57\%$). So, the volume increases aproximately 2%, which corresponds to a thermal expansion coefficient of $\alpha = 4.02 \times 10^{-5}$ K^{-1}, similar to that reported for $LaCrO_3$-based perovskites.[23] Thus, we may conclude that this electrical response is not due to any structural change.

An Arrhenius-type plot of the resistivity shows this region of the PTC as a negative slope region in Figure 7. The slope increases with the La content. Typically, we correlate this increase with a higher concentration of donors, but further

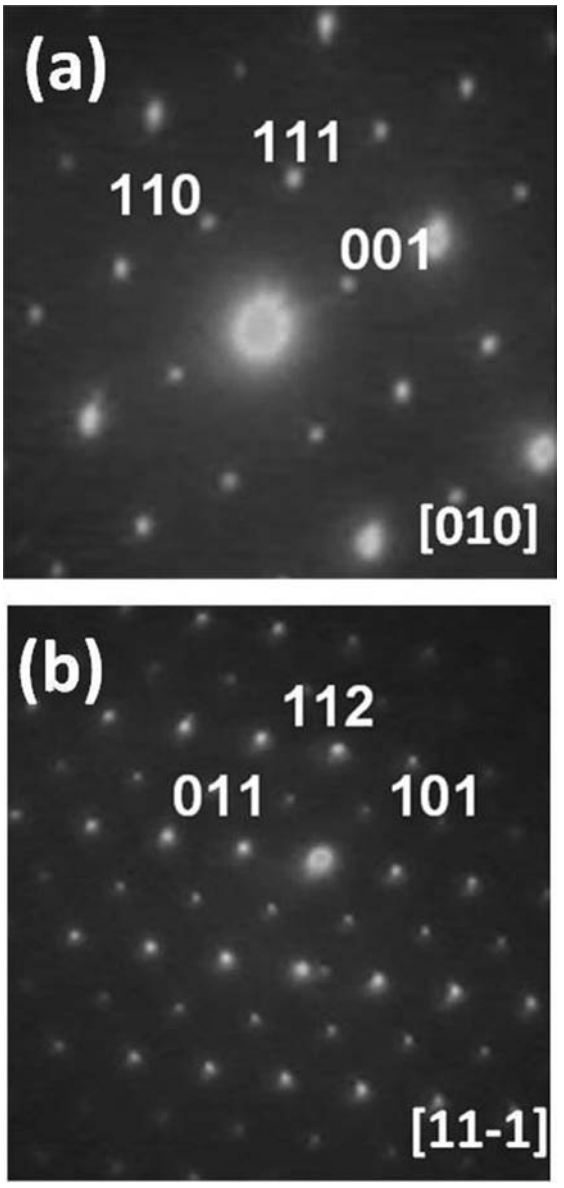

Figure 4. SAED patterns of $Bi_{0.5}La_{0.5}Fe_{05}Cr_{0.5}O_3$: (a) zone axis [1−10]; (b) zone axis [11−1].

studies may be done to separate both the semiconductor and dielectric effects. The election of different frequencies for plotting the conductivity (1 kHz) and permittivity (1 MHz), respectively, optimizes the electrical response in each case because of the frequency dependence of the admittance $Y = 1/Z$. This magnitude may be represented, for a sample with an electrode surface, S, and a thickness, t, as $Y = 1/R + i\omega C$, where the resistance R corresponds to $t/S\rho$ and the capacitance is a complex magnitude related to the permittivity as follows: $C = S/t(\varepsilon_R - i\varepsilon_I)$. As we can easily see, the part of the admittance due to permittivity is more important at higher frequencies. However, we obtained better results for the part corresponding to the conductivity (reciprocal resistivity) at lower frequencies.

The origin of the semiconductor response may correspond to substitution on the A site (La/Bi), as can be seen in Figures 5 and 6, something also reported for Ln/Ba substitution in $BaTiO_3$ by several authors.[24,25] Semiconductors with PTC may not be

dx.doi.org/10.1021/ic2008864 |*Inorg. Chem.* 2011, 50, 8340–8347

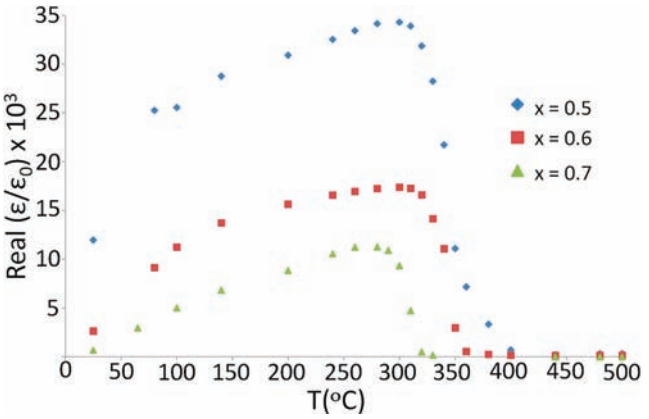

Figure 5. Real part of the normalized permittivity as a function of the temperature and measured at 1 MHz for several members of the solid solution.

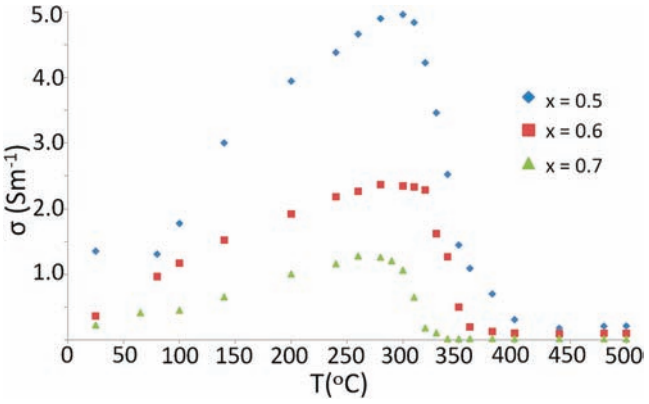

Figure 6. Electrical conductivity versus temperature measured at 1 kHz for several members of the solid solution.

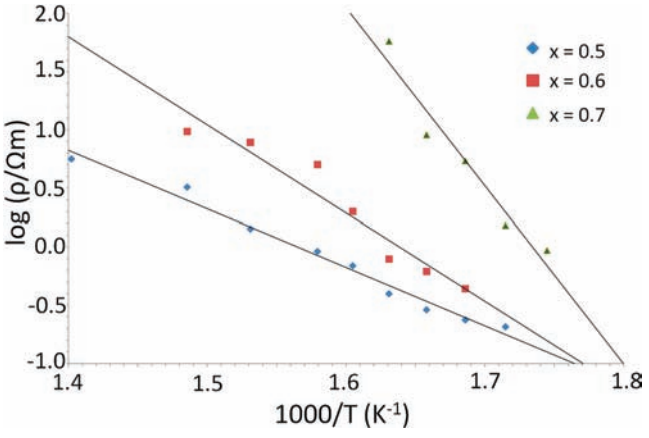

Figure 7. Arrhenius-type plot of resistivities of different members of the solid solution.

single crystals but polycrystalline ceramics, and in this case, some authors[26] have proposed this phenomenon to originate in the Schottky barrier at the grain boundaries. In the temperature range corresponding to this phase transition, we find that resistivity increases with increasing temperature in several orders of magnitude. Another, quite different, mechanism regarding the

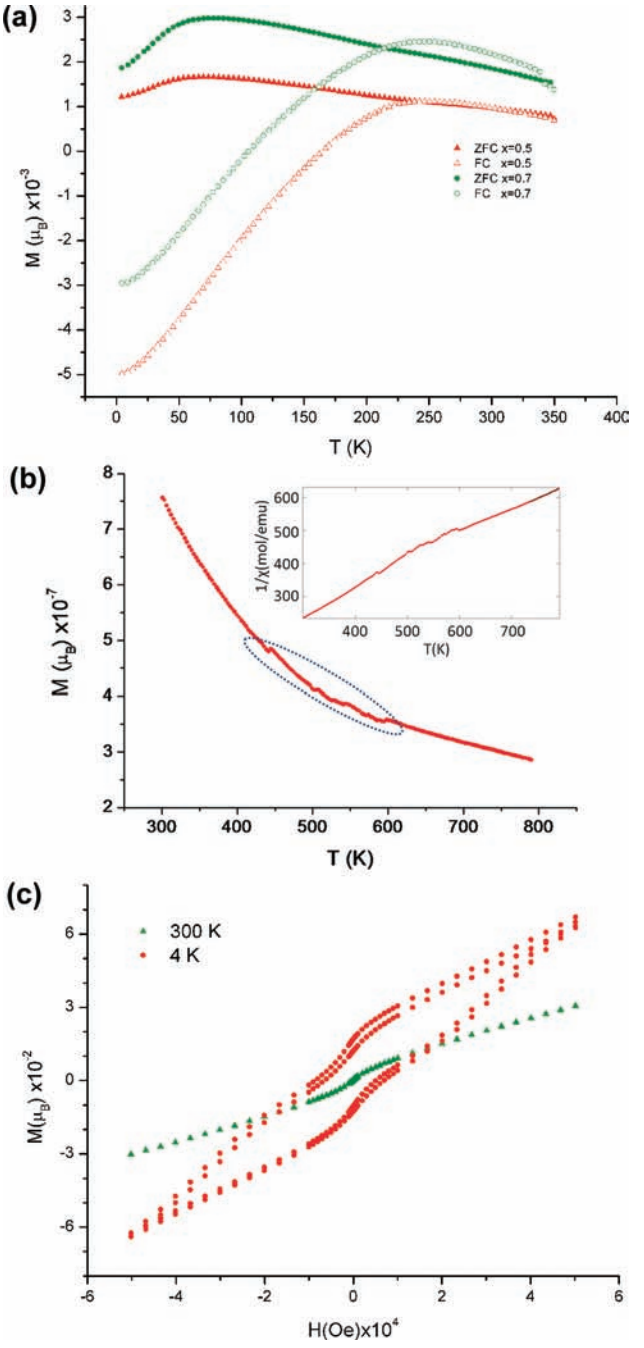

Figure 8. (a) Magnetic vs T plots for the $x = 0.5$ and 0.7 samples. ZFC and FC curves appear inverted. (b) Magnetic vs T plot for the $x = 0.5$ sample in the high-temperature (paramagnetic) region. Magnetic anomalies, probably related to the PTC electric behavior, are highlighted. The inverse susceptibility is plotted in the inset to show the Curie–Weiss behavior. (c) Magnetization vs magnetic field at 5 K measured for the $x = 0.7$ sample. The hysteresis plot shows some exchange-bias behavior.

change toward more metallic character in the PTC region could be a Franck–Condon charge transfer from Fe^{3+} to Cr^{3+}, as reported for $LaFe_{1-x}Cr_xO_3$ materials.[27] If this mechanism were predominant, strong electron–phonon interactions would be very important, lattice mediated, directly affected by the temperature and could indirectly be affected by substitutions in the A site (La/Bi) also. None of these possible mechanisms excludes

dx.doi.org/10.1021/ic2008864 |Inorg. Chem. 2011, 50, 8340–8347

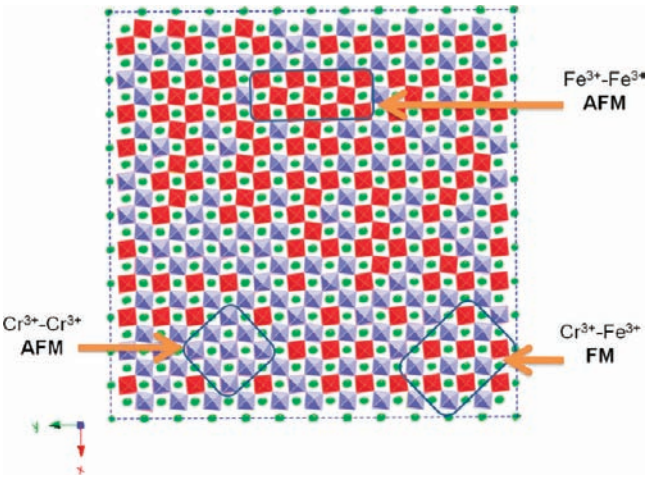

Figure 9. Magnetic microdomains in $La_xBi_{1-x}Fe_{0.5}Cr_{0.5}O_3$ ($0.4 \leq x \leq 1$) materials.

each other, and an adequate explanation for this complex behavior needs further study.

e. Magnetic Properties. Figure 8a shows the temperature dependence of the magnetic magnetization, M, for several samples. The measurements were done according to the following protocol: First, the as-prepared samples were cooled from room temperature to 4 K with no applied field; the ZFC temperature-dependent magnetization was then measured in an applied field H = 0.1 T with increasing temperature; subsequently, the samples were demagnetized at room temperature and cooled again with H = 7 T; finally, the FC magnetization was recorded in an applied field H = 0.1 T. Figure 8b shows the high-temperature behavior of the susceptibility, and the inverse susceptibility is plotted in the inset. Several features are already apparent. Large irreversibilities between the ZFC and FC runs develop as the temperature is decreased, pointing out that magnetic frustration and disorder not only are present but also dominate the magnetic properties in the system. This is expected because of the random positioning of Fe and Cr atoms in the sublattice B (antisite disorder); interestingly enough, ZFC data, systematically and almost in the whole temperature range explored, lie above the corresponding FC runs, with the latter rendering even negative values of the magnetic moment at low temperatures. This behavior very much resembles that reported by Azad et al.[3] for $LaFe_{0.5}Cr_{0.5}O_3$, and it is understood in terms of the presence of a nonnegligible amount of uncompensated spins within an overall AFM scenario. Within this picture, the broad maximum in the FC runs would signal the onset of the antiferromagnetic transition, TN around 260 K. In order to further check the presence of uncompensated spins, we measured the hysteresis cycles at 4.2 K under two conditions. First, starting with an as-prepared sample, we cooled the system in no applied field to 4.2 K and measured the cycle at 4.2 K; second, we warmed the sample at room temperature and cooled it to 4.2 K again in a 7 T field to finally measure the corresponding loop at 4.2 K. We proceeded in that manner because exchange bias occurs in systems where a ferromagnet shares an interface with a larger magnetic anisotropy antiferromagnet, so the latter can pin the orientation of the FM component below the Néel temperature. Given the large number of interfaces intimately connecting the AFM d^3-d^3 (Cr^{3+}/Cr^{3+}) and d^5-d^5 (Fe^{3+}/Fe^{3+}) antisite disorder patches with FM Cr^{3+}/Fe^{3+} islands, exchange-bias effects are expected. Figure 8c shows a representative set of ZFC and FC cycles for the $La_{0.7}Bi_{0.3}Fe_{0.5}Cr_{0.5}O_3$ sample. Large offsets (vertical shifts) for the ZFC and FC hysteresis loops are already seen. This points to the existence of a spin-glass-like system, corresponding to a highly disordered AFM matrix, conformed by the d^3-d^3 (Cr^{3+}/Cr^{3+}) and d^5-d^5 (Fe^{3+}/Fe^{3+}) antisite disorder patches, and some FM islands, corresponding to the ferromagnetic Cr^{3+}/Fe^{3+} patches, as schematized in Figure 9. Antiphase boundaries in the AFM matrix can also be an additional source of uncompensated spins. The large coercivity observed matches well with the large magnetic frustration present in these disordered systems because a large coercive force is necessary to bring the thermoremanent magnetization to zero.

CONCLUSION

A new solid solution, $La_xBi_{1-x}Fe_{0.5}Cr_{0.5}O_3$ ($0.4 \leq x \leq 1$), featuring the perovskite structure has been prepared and characterized. The transport properties are as peculiar as they are interesting: a PTC has been found in the electrical resistivity at moderate temperatures (270−400 °C), and regarding the magnetic properties, they are anomalous because all samples show ZFC curves over the FC ones, which is interpreted on the basis of interacting microdomains with different Fe/Cr compositions and different FM or AFM character.

AUTHOR INFORMATION

Corresponding Author

*E-mail: emoran@quim.ucm.es.

Present Address

[▽]Departamento de Electrocerámica, Instituto de Cerámica y Vidrio, CSIC, Cantoblanco, 28049, Madrid, Spain.

ACKNOWLEDGMENT

M.E.V. is indebted to DGAPA, UNAM, for granting her a sabbatical year at the Universidad Complutense in Madrid. Financial support from different projects made this work possible and is consequently acknowledged: PAPIIT-UNAM Project IN116610-3, UPM Project AL08-P(I+D)-20, Spanish Ministery for Science Projects MAT-2007-64006, CSD2009-00013, and MAT2008-06517-C02-01, and CAM (Autonomous Community of Madrid) Program S-0505/PPQ/0358. The authors also gratefully thank Drs. Julian Velázquez, Emilio Matesanz, and Fernando Conde (UCM Center for X-ray Diffraction) for technical support and Dr. Dos Santos-García (UCM) for careful reading of this manuscript.

REFERENCES

(1) Kanamori, J. *J. Phys. Chem. Solids* **1959**, *10*, 87–98.
(2) Goodenough, J. B. *Phys. Rev.* **1955**, *100*, 564–573.
(3) Azad, A. K.; Mellergård, A.; Eriksson, S. G.; Ivanov, S. A.; Yunus, S. M.; Lindberg, F.; Svensson, G.; Mathieu, R. *Mater. Res. Bull.* **2005**, *40*, 1633–1644.
(4) Dahmani, A.; Taibi, M.; Nogues, M.; Aride, J.; Loudghiri, E.; Belayachi, A. *Mater. Chem. Phys.* **2002**, *77*, 912–917.
(5) Ueda, K.; Tabata, H.; Kawai, T. *Science* **1998**, *280*, 1064.
(6) Baettig, P.; Spaldin, N. A. *Appl. Phys. Lett.* **2005**, *86*, 012505.
(7) Spaldin, N. A.; Fiebig, M. *Science* **2005**, *309*, 391.
(8) Suchomel, M. R.; Thomas, C. I.; Allix, M.; Rosseinsky, M. J.; Fogg, A. M. *Appl. Phys. Lett.* **2007**, *90* (11), 112909.

(9) Li, J. B.; Rao, G. H.; Liang, J. K.; Liu, Y. H.; Luo, J.; Chen, J. R. *Appl. Phys. Lett.* **2007**, *90*, 162513.
(10) Guo, H. Y.; Chen, J. I. L.; Ye, Z. G. *J. Mater. Res.* **2007**, *22* (8), 2081–2086.
(11) Chen, J. R.; Wang, W. L.; Li, J. B.; Rao, G. H. *J. Alloys Compd.* **2008**, *459*, 66–70.
(12) Bashir, A.; Ikram, M.; Kumar, R.; Thakur, P.; Chae, K. H.; Choi, W. K.; Reddy, V. R. *J. Phys.: Condens. Matter* **2009**, *21*, 325501.
(13) Singh, R. P.; Tomy, C. V. *J. Phys.: Condens. Matter* **2008**, *20*, 235209.
(14) Wersing, W. Ferroelectric Ceramics. In *Ferroelectric devices*; Setter, N., Colla., E. L., Eds.; Birkhaüser: Berlin, 1993.
(15) Rodríguez-Carvajal, J.. Abstracts of the Satellite Meeting of the 15th Congress of the IUCr, Toulouse, France, 1990; p 127 (http://www.ill.eu/sites/fullprof/).
(16) Blasco, J.; Stankiewicz, J.; Garcia, J. *J. Solid State Chem.* **2006**, *179* (3), 898–908.
(17) Oikawa, K.; Kamiyama, T.; Hashimoto, T.; Shimojyo, Y.; Morii, Y. *J. Solid State Chem.* **2000**, *154*, 524–529.
(18) Marezio, M.; Dernier, P. D. *Mater. Res. Bull.* **1971**, *6*, 23–30.
(19) Reyes, A.; de la Vega, C.; Fuentes, M. E.; Fuentes, L *J. Eur. Ceram. Soc.* **2007**, *27*, 3709–3711.
(20) Shannon, R. d.; Prewitt, C. T. *Acta Crystallogr.* **1969**, *B25*, 925.
(21) Ihrig, H.; Hennings, D. *Phys. Rev. B* **1978**, *17*, 4593–4599.
(22) Shiosaki, T.; Takeda, H.; Goto, R.; Kinshita, T.; Shimada, T.; Katsuyama, Y. *Proc. 2006 IEEE Int. Symp. Appl. Ferroelectr., 15th* **2006**, 193–196.
(23) Zuev, A.; Singheiser, L.; Hilpert, K. *Proc. Int. Symp. Solid Oxide Fuel Cells, 8th* **2003**, *7*, 817–831.
(24) Ihrig, H.; Hennings, D. *Phys. Rev. B* **1978**, *17*, 4593–4599.
(25) Chang, F.; Zhang, N. Y.; Wang, S.; Song, G. *J. Phys. D: Appl. Phys.* **2007**, *40*, 7799–7803.
(26) Heywang, H. *J. Mater. Sci.* **1971**, *6*, 1214.
(27) Andreasson, J.; et al. *Phys. Rev. B* **2007**, *75*, 104302.